Low-cost shrink lithography with sub-22 nm resolution

Cite as: Appl. Phys. Lett. **100**, 133113 (2012); https://doi.org/10.1063/1.3697836
Submitted: 25 December 2011 . Accepted: 13 February 2012 . Published Online: 30 March 2012

Bo Zhang, Min Zhang, and Tianhong Cui

Low-cost shrink lithography with sub-22 nm resolution

Bo Zhang,[a] Min Zhang,[a] and Tianhong Cui[b]
Department of Mechanical Engineering, University of Minnesota, 111 Church Street S.E., Minneapolis, Minnesota 55455, USA

(Received 25 December 2011; accepted 13 February 2012; published online 30 March 2012)

A low-cost shrink lithogragphy technique with 21 nm resolution is presented in this paper. The shrink lithography uses embossing approach to pattern the heat-shrink polymer film, and thermally shrink the film as a shadow mask subsequently. Metal patterns with diffferent feature sizes were achieved from a single mold by shrink lithography through controlling the shrink contidions including temperature and force. A biosensor based on a suspended graphene nanoribbon is fabricated with the shrink lithography, demonstrating the potential application of this process to the fabrication of nanodevices and integrated circuits. © *2012 American Institute of Physics*. [http://dx.doi.org/10.1063/1.3697836]

Lithography is playing an important role in many areas of modern science and technology, including the production of integrated circuits, information storage devices, microelectromechanical systems, microfluidic devices, biochips.[1–5] The dimension of pattern feature on a chip has been decreased steadily for several decades, driven by a combination of market forces and technological innovation. The continuous development of low cost and smaller pattern scale lithography techniques are essential for the semiconductor integrated circuits and nanodevices to reach the intrinsic technological and economical limits. Numerous nano scale fabrication techniques are under development to touch next milestone of semiconductor industry. Scanning electron beam lithography has demonstrated sub-10 nm resolution,[6] however, it requires pixel-by-pixel patterning in a serial manner, which greatly increases the cost and prevents from its economical practice for mass production. Nanoimprinting technique has demonstrated sub-25 nm resolution,[7] however, its mold fabrication cannot avoid electron beam lithography, which introduces high cost as well. Copolymer lithography is also capable of offering sub-25 nm resolution,[8] but it suffers from the limitation of pattern variety due to the copolymer properties. To overcome the hurdles of the previous nano scale fabrication methods, a low-cost lithographic method based on thermoplastics and embossing molding is presented in this report. The shrink lithography demostrated here is capable of achieving sub-22 nm patterns without any expensive nano fabrication such as electron beam lithography.

Thermoplastics are attracting more and more attentions in micro/nano fabrication in recent years.[9–11] Depending on resin selection and blend proportion, these thermoplastics can shrink by varying amounts when heat is applied.[12] Molding is a low cost and high throughput mean to replicate functional and artisanal patterns.[13,14] However, the molds are very expensive to create and control at nanoscale dimension.[15] Herein, shrink lithography combines the thermoplastic film with hot embossing molding process to successfully achieve 21 nm metal lines and large scale array patterns. In addtion, a suspended graphene nanoribbon biosensor was fabricated by using shrink lithography, demonstrating that shrink lithography has the potential to become a commercially viable lithography for the manufacture of nanoscale structure.

The procedure of shrink lithography is outlined in Fig. 1(a). In shrink lithography, as is shown in Fig. 1(b), a typical mold was first prepared by conventional photolithography, potassium hydroxide (KOH) etching, and subsequent eletroplating. In order to get sharp tips on molds, anisotropic etching of silicon wafer is a low-cost and simple way. However, the silicon wafer is not suitable for hot embossing because it is brittle with a short lifetime. On the other hand, Ni mold can be used for many times without deformation of molding patterns. In addition, electroplating technique is also an inexpensive fabrication method, thus we use electroplating method to fabricate a Ni mold instead of a silicon mold. In the following embossing molding steps, the mold was embossed against the shrink film and held for 2 min. The shrink film (Sealed Air Nexcel

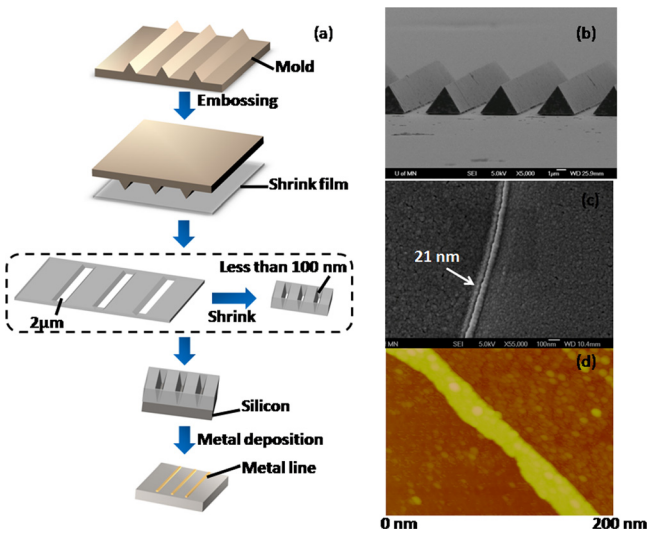

FIG. 1. (a) Sketch of shrink lithography processes. The shrink lithography uses embossing molding method to pattern the shrink film, and thermally shrink the film as a shadow mask subsequently. Metal patterns are obtained by sputtering. SEM images of (b) mold and (c) 21 nm line. (d) AFM image of 21 nm line.

[a]Bo Zhang and Min Zhang contributed equally to this work.
[b]E-mail: tcui@me.umn.edu. Tel.: 612-626-1636.

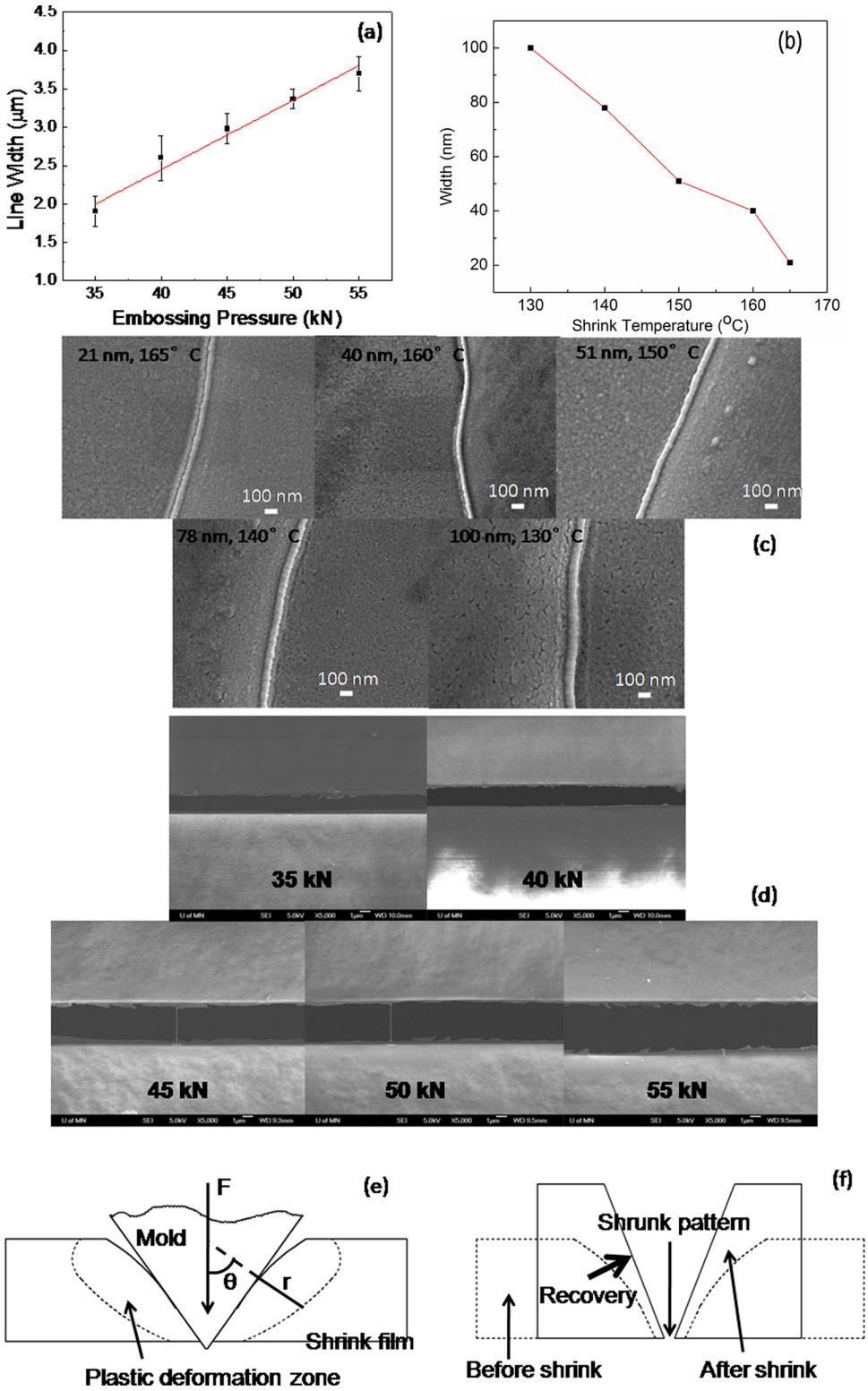

FIG. 2. (a) Shift in groove width versus embossing pressure for shrink lithography. Width of the grooves raises with the increase of embossing press when the operating temperature is controlled at room temperature. (b) Line width versus shrink temperature under the condition of controlling the embossing press at 50 kN. Width of the metal lines decreased with the rising of the temperature. (c) SEM images of the metal lines fabricated by shrink lithography from the same mold at different shrink temperatures. (d) SEM images of the grooves embossed by the mold with the increase of embossing press when the operating temperature is controlled at room temperature. (e) A load on the mold positioned onto the shrink film causes local plastic deformation below the tips around. and (f) The recovery of shrink film will decrease the width of the patterns greatly.

multilayer shrink film 955D) comprising 5 layers of co-extruded polyolefin (PO) 7 μm thick was purchased from SealedAir. After that, release the mold, and PO shrink film with impenetrated patterns was obtained. The feature size of the impenetrated patterns was controlable by appling different embossing pressure. Next, the patterned PO shrink film was placed between two silicon wafers for uniform heating. The samples were heated to desired temperature in a slowly rising process for approximately 5 min, and held for 10 min for shrinking in a convection oven. This slow heating process with assistance of two silicon wafers facilitated the uniform shrinkage of the PO shrink film with minimum of deformations. Due to the adhesion of shrink polymer film at high shrink temperature, the PO shrink film bonded with silicon substrate very well, acting as a shadow mask for metal deposition. Finally, chrome was depostied on the substrate by sputtering. As is shown in Fig. 1(c), a 21 nm line pattern was fabricated by this shrink lithography.

In the meanwhile, most current molding methods have a common goal that is to generate replicas of the molds. Therefore, if different features of pattern are desired, new molds are necessary to create for every new pattern, which is very high-cost. However, shrink lithography is capable of generating various feature sizes of patterns from a single mold according to controlling the embossing pressure and shrink temperature. Therefore, the material and shrinkage properties of these films are characterized under different embossing pressure and shrink temperatures. As is shown in Fig. 2(a), the width of the grooves embossed by the mold raises with the increase of embossing press when the operating temperature is controlled at room temperature. Besides, by controlling the embossing press at 50 kN, the width of metal lines fabricated by shrink lithography from the same mold were characterized at different shrink temperatures. As is shown in Fig. 2(b), the width of the metal lines decreased with the rising of the temperature. SEM images of these samples were taken and demonstrated this trend clearly in Figs. 2(c) and 2(d), respectively. As was reported in the previous literature,[9,16] the PO shrink films can shrink reproducibly up to 95% in area. However, our shrinkage results are from several micrometer down to sub-100 nm, which is much larger. The reason is that the thermal recovery property of PO shrink film enhances the shrinkage of impenetrated patterns. As is shown in Fig. 2(e), applying a load on the mold positioned onto the PO shrink film will initially cause local plastic deformation below the tips around cutting wedge of impenetrated patterns. This deformation depends on the load necessary for indentation, the elastic modulus of shrink film and the local shear stresses under the wadge.[17] Based on the appropriate boundary conditions, a general solution for linear elastic stresses supporting the applied cutting force yields a solution for shear stress τ

$$\tau = -\frac{F\cos\theta}{\pi r}, \tag{1}$$

where F is the wedge force per unit thickness, r is the distance from the wedge to the point under consideration, and θ is the angle measured from the direction of the force.[18,19] If these shear stresses exceed the shear strength of shrink film, delamination will occur.[20] Thus, the plastic deformation zone size R can be derived from the equation above with r = R. Due to the thermal recovery property of PO shrink film, the matter squeezed aside next to the wedge will attend to recover to its initial shape before embossing[21] when heat is applied. As is shown in Fig. 2(f), this recovery of PO shrink film will sharpen the grooves width greatly, combining with the intrinsic shrinkage of PO film, to offer the extremely large shrink ratio. In principle, the vertical dimension of the mold patterns will be used to define the range of the film thickness. By adjusting the temperature and press, the impenetrated patterns can be obtained in the film, and the pattern thickness is equal to or less than the vertical dimension of the patterns on the mold. However, thicker films will get more local plastic deformation. After the thermal recovery, the material squeezed aside next to the wedge will recover to its initial shape, and this will seal the generated patterns in the thicker shrink film, resulting in a lower yield.

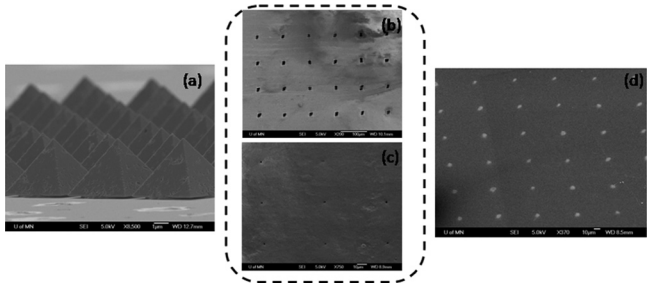

FIG. 3. SEM images of (a) dot array mold, (b) film before shrink, (c) film after shrink, and (d) metal dot array.

Therefore, thiner shrink film will have higher yield rate of the nanofabrication process. In addtion, as is shown in Fig. 3, the large scale array patterns manufactured by shrink lithography were also demonstrated.

Graphene nanoribbon patterned from shrink lithography were also successfully used to fabricate suspended prostate specific antigen (PSA) cancer biosensor, revealing the practical application potential of this shrink lithography. Graphene has attracted more and more attentions due to its unique structural, electrical, chemical, and mechanical properties, especially its two dimensional structure which is perfectly compatible with lithography.[22,23] In the meanwhile, graphene nanoribbons have emerged as an interesting material with a wealth of electronic and spin transport properties, such as open-up band gaps of graphene.[24–26] With the shrink lithography technique, the shrunk ultra-narrow patterns were transferred to the graphene fabricated by mechanical exfoliation. The graphene nanoribbons were generated at a level of 50 nm width. We started with a graphene plate genearated by mechanical exfoliation method on a SiO_2/Si wafer.[27] Next, by shrink lithography process, the shrunk film with narrow groove pattern was as a shadow mask on the top of graphene. Atomic layer deposition was used to deposit a layer of Al_2O_3 8 nm thick. Next, the shrink film was stripped, and oxygen plasma was applied to pattern the graphene nanoribbon. Sequentially, gold electrodes were sputterred, and buffered HF was introduced to etch away the SiO_2 layer, followed by super critical drying to release the suspended graphene nanoribbon structure (Figs. 4(c) and 4(d)). Next, anti-PSA antibodies as bioreceptors were immobilized on the graphene nanoribbon to test the PSA.[28] The detection mechanism of the biosensor is illustrated in the inset of Fig. 4(e). Given that the conductance of graphene is proportional to the product of charge carrier density and mobility,[29,30] it is believed that changes in density and/or mobility of charge carriers must be responsive when PSA are captured by the antibodies modified on a graphene nanoribbon. The equation, $\sigma = nq\upsilon$, can show the relationship clearly, where σ is conductance, n is carrier density, q is charge per carrier, and υ is the carrier mobility. As is shown in Fig. 4(e), the conductance-versus-time measurements recorded on the graphene nanoribbon biosensor in both suspended and unsuspended situations demonstrated the good perfermance of detection of PSA. The suspended biosensor showed better detection limits (1 pg/ml) than the unsuspended one (10 pg/ml) due to the enhanced signal to noise ratio in the suspended graphene.[31]

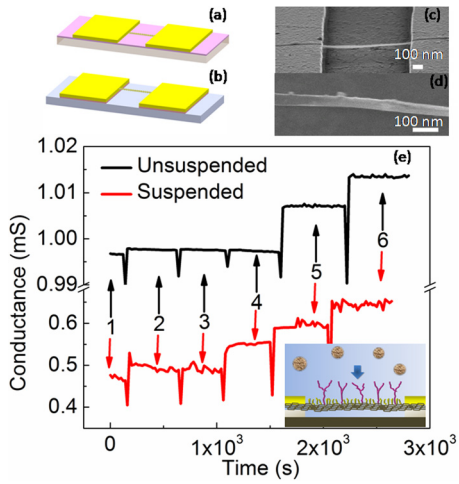

FIG. 4. Sketches of (a) unsuspended and (b) suspended graphene nanoribbon. (c) SEM images of suspended grapheme nanoribbon. (d) High magnitude SEM image of graphene nanoribbon. (e) The detection limit results of graphene nanoribbon based biosensor in both suspended and unsuspended situations. Conductance versus time data recorded after alternate delivery of the following concentrations of PSA: (1) PBS contains no PSA, (2) 0.1 pg/ml, (3) 1 pg/ml, (4) 10 pg/ml, (5) 1 ng/ml, and (6) 1 μg/ml. Inset: the illustration of PSA sensing mechanism, where the graphenenanoribbon is modified with PSA antibody receptors. PSA bonded specifically to receptors will produce a conductance change of the graphene nanoribbon.

The shrink lithography offers a number of advantages over the current conventional lithography techniques. The shrink lithography achieves very low cost process in manufacturing nanoscale patterns without any expensive technique such as electron beam lithography. The embossing molding of shrink lithography is capable of patterning large area at once, which offers the oppotunity of mass production. In addition, different feature sizes of patterns can be realized by shrink lithography from a single mold by controlling the embossing pressure and shrink temperatures, which introduces a programable lithography and further decreases the cost. We believe that sub 10 nm shrink lithography will be achievable with a further development such as optimization of shirnk temperature and embossing pressure as well as improvement of shrink film materials.

The authors acknowledge the assistance of fabrication and characterization from Nanofabrication Center and the Characterization Facility at the University of Minnesota. The authors also thank Dr. Min Zhang for his help in taking SEM images.

[1]T. Ito and S. Okazaki, Nature **406**, 1027 (2000).
[2]T. Sekitani, T. Yokota, U. Zschieschang, H. Klauk, S. Bauer, K. Takeuchi, M. Takamiya, T. Sakurai, and T. Someya, Science **326**, 1516 (2009).
[3]D. Lee and T. Cui, Biosens. Bioelectron. **25**, 2259 (2010).
[4]K. Handique, D. T. Burke, C. H. Mastrangelo, and M. A. Burns, Anal. Chem. **72**, 4100 (2000).
[5]M. Yue, J. C. Stachowiak, H. Lin, R. Datar, R. Cote, and A. Majumdar, Nano Lett. **8**, 520 (2008).
[6]P. Fischer and S. Chou, Appl. Phys. Lett. **62**, 2989 (1993).
[7]S. Chou, P. Krauss, and P. Renstrom, Science **272**, 85 (1996).
[8]I. Bita, H. Kang, F. A. Detcheverry, E. Dobisz, D. S. Kercher, T. R. Albrecht, J. J. de Pablo, and P. F. Nealey, Science **321**, 939 (2008).
[9]D. Nguyen, D. Taylor, K. Qian, N. Norouzi, J. Rasmussen, S. Botzet, M. Lehmann, K. Halverson, and M. Khine, Lab Chip **10**, 1623 (2010).
[10]K. Sollier, C. A. Mandon, K. A. Heyries, L. J. Blum, and C. A. Marquette, Lab Chip **9**, 3489 (2009).
[11]C. Hong, H. Maeng, K. Song, and S. Kaang, J. Appl. Polym. Sci. **112**, 886 (2009).
[12]A. Torres, N. Colls, and F. Mendez, J. Plast. Film Sheeting **22**, 29 (2006).
[13]M. Lee, M. D. Huntington, W. Zhou, J. Yang, and T. W. Odom, Nano Lett. **11**, 311 (2011).
[14]M. Heckele and W. Schomburg, J. Micromech. Microeng. **14**, R1 (2004).
[15]F. Huo, Z. Zheng, G. Zheng, L. R. Giam, H. Zhang, and C. A. Mirkin, Science **321**, 1658 (2008).
[16]D. Taylor, D. Dyer, V. Lew, and M. Khine, Lab Chip **10**, 2472 (2010).
[17]N. Stutzmann, T. A. Tervoort, K. Bastiaansen, and P. Smith, Nature **407**, 613 (2000).
[18]R. Meehan and S. Burns, ASME J. Manuf. Sci. Eng. **129**, 477 (2007).
[19]R. Meehan and S. Burns, Exp. Mech. **38**, 103 (1998).
[20]R. Hill, E. Lee, and S. Tupper, Proc. R. Soc. London Ser. A **188**, 273 (1947).
[21]X. Liu, A. Chakraborty, and C. Luo, J. Micromech. Microeng. **20**, 095025 (2010).
[22]K. S. Novoselov, A. K. Geim, S. V. Morozov, D. Jiang, Y. Zhang, S. V. Dubonos, I. V. Grigorieva, and A. A. Firsov, Science **306**, 666 (2004).
[23]Y. Ohno, K. Maehashi, Y. Yamashiro, and K. Matsumoto, Nano Lett. **9**, 3318 (2009).
[24]X. Wang and H. Dai, Nat. Chem. **2**, 661 (2010).
[25]L. Jiao, L. Zhang, L. Ding, J. Liu, and H. Dai, Nano Res. **3**, 387 (2010).
[26]A. Sidorov, T. Bansal, P. J. Ouseph, and G. Sumanasekera, Nanotechnology **21**, 195704 (2010).
[27]P. Li, Z. You, G. Haugstad, and T. Cui, Appl. Phys. Lett. **98**, 253105 (2011).
[28]B. Zhang and T. Cui, Appl. Phys. Lett. **98**, 073116 (2011).
[29]F. Schedin, A. K. Geim, S. V. Morozov, E. W. Hill, P. Blake, M. I. Katsnelson, and K. S. Novoselov, Nature Mater. **6**, 652 (2007).
[30]E. H. Hwang, S. Adam, and S. Das Sarma, Phys. Rev. B **76**, 195421 (2007).
[31]Z. Cheng, Q. Li, Z. Li, Q. Zhou, and Y. Fang, Nano Lett. **10**, 1864 (2010).